Operation scheme for MMC-based STATCOM using modified instantaneous symmetrical components

Qing DUAN*, Wanxing SHENG, Guanglin SHA, Zhen LI, Caihong ZHAO, Penghua LI, Chunyan MA
Key Laboratory of Distribution Transformer Energy-Saving Technology (China Electric Power Research Institute), Beijing, P.R. China

Abstract: Modular multilevel converters (MMCs) are characterized by modularization and multielectric equality, and the application of this structure to a high-voltage large-capacity static synchronous compensator (STATCOM) shows good potential. In this paper, a modified instantaneous symmetrical component method is proposed for positive- and negative-sequence decomposition, i.e. the critical part of the control device, which can accurately detect the instantaneous value of each sequence component in three-phase asymmetrical phasors in real time. Then, based on this method, the paper proposes a control method for MMC-based STATCOMs that solves the problems of multi-DC (direct current) voltage balance, grid-connected current control, and circulation suppression. Finally, the proposed detection and control methods are verified by performing simulations and experiments. The results show that the proposed method can quickly and accurately detect the positive- and negative-sequence reactive component that should be compensated by the device, thus realizing real-time reactive compensation for MMC-based STATCOMs.

Key words: MMC, STATCOM, modified instantaneous symmetrical components, unbalance compensation

1. Introduction

With the development of power systems, a large number of reactive loads results in grids with low power factors. In addition, unbalanced loads result in unbalanced three-phase grids [1–3], which have a negative impact on the stability, safety, and economical operation of power grids. The use of static synchronous compensators (STATCOMs) can effectively increase the system power factor and improve the voltage level, which is an important component of flexible AC transmission systems (FACTS) [4, 5]. With the increased scale of power systems, there are greater requirements with respect to the capacity and voltage class of compensation devices. Therefore, the development of STATCOMs with high voltage and high power is an inevitable trend [6, 7].

The structures of modular multilevel converters (MMCs) are highly modular. By increasing the number of power units, the main circuit can be expanded, and the output level is large, having a small influence on the harmonic wave of AC networks [8–10]. In addition to realizing flexible DC transmission, MMCs can also be used as STATCOMs in the field of power-quality control [11]. MMCs have been used extensively in flexible DC transmission systems and have yielded a series of research results. However, the application of MMCs to the field of power quality is still in the initial stages, and there is an urgent need for additional research. The focus of the present paper is STATCOM-based MMCs, and a control method was designed for the working condition

---

*Correspondence: duanqing_epri@163.com

of the reactive power. Experimental results show that MMC-based STATCOMs can realize flexible reactive power control, but a detailed control method is not illustrated.

Positive-sequence and negative-sequence decomposition is a significant link of STATCOMs. The traditional symmetrical component method is a three-phase asymmetrical system analysis method that is based on the steady state, while the instantaneous symmetrical component method adopts the instantaneous value of the three-phase asymmetrical variable in order to perform the symmetrical component transformation [12–14]. Thus, it can be used in the dynamic and transient analysis of three-phase asymmetrical systems. However, most of the literature represents the sequence components of the three-phase asymmetrical variable in the plural or differential form, and a 90° phase shift should be conducted to obtain the instantaneous value of sequence components during the transformation. It is not possible to represent the instantaneous value in a real scenario.

The design method of the hardware parameters and controller of MMCs has been studied in [15-19], but these methods cannot be directly applied to reactive power compensation control of the MMC-based STATCOM. In the present paper, we propose a modified instantaneous symmetrical component transformation method. We use a two-point sampling method according to the corresponding relation between the rotation phasor and its instantaneous value in two-dimensional time-domain orthogonal coordinates. Moreover, it further designs the control method of multi-DC voltage, positive- and negative-sequence current, and circulating-current restraint of MMC-based STATCOMs. Finally, we verify the results by performing simulations and experiments.

2. Structure of MMC-based STATCOM

The topology structure of the proposed MMC-based STATCOM is as shown in Figure 1. The submodule is composed of half-bridge and DC capacitance. Each phase consists of upper and lower bridge arms, which are in parallel in the common DC bus. Each bridge arm is connected by N power unit submodules and a bridge arm reactor L. The equivalent circuit diagram of the MMC main circuit is as shown in Figure 2. L_s and R_s indicate the equivalent reactance and resistance, respectively, on the AC side and e_{sj} and i_{sj} are the voltage and current, respectively, of the AC side. L refers to the bridge-arm inductance. u_{pj} and u_{nj} refer to voltages of the upper and lower bridge arms, respectively, i_{pj} and i_{nj} are the currents in the upper and lower bridge arms, respectively, and j represents the a, b, and c phases.

With respect to the bridge-arm current, in addition to the AC-side output current component, there is a part i_{zj} that circulates only in the bridge arm. This component does not output active power to the AC side. According to Kirchhoff's current law, the loop current in the j phase can be represented by the bridge-arm current.

$$i_{zj} = \frac{1}{2}(i_{pj} + i_{nj}) \tag{1}$$

The AC-side output current is

$$i_{sj} = i_{nj} - i_{pj} \tag{2}$$

According to Eq. 2, the MMC AC-side output current is related only to the difference between the upper and lower bridge-arm currents. The required AC output current can be obtained by controlling the upper and lower bridge-arm current using a specific control strategy.
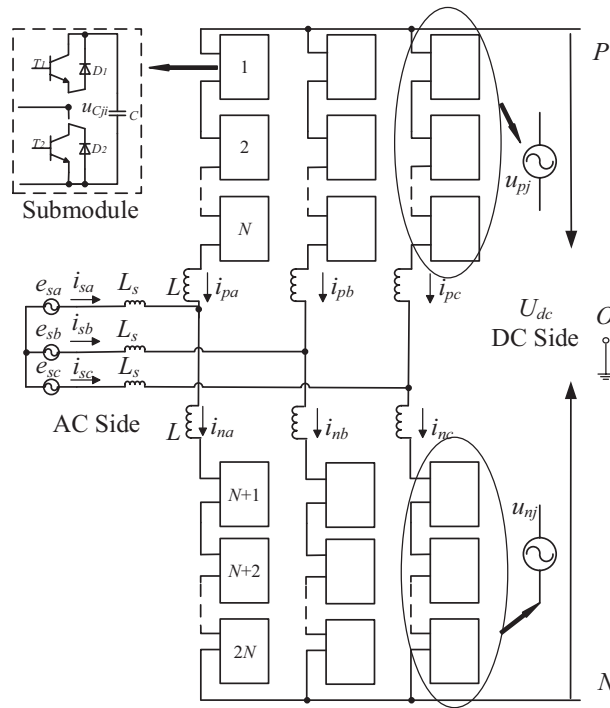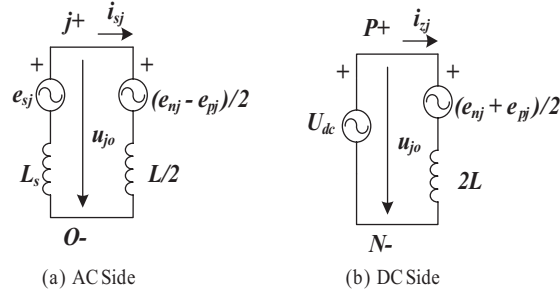
Figure 1. Topology structure of MMC-based STATCOM.

(a) AC Side

(b) DC Side

Figure 2. Equivalent MMC circuit model.

According to Kirchhoff's current law, it can be concluded that

$$\frac{u_{nj} - u_{pj}}{2} = e_s - (\frac{L}{2} + L_s)\frac{di_{sj}}{dt} \tag{3}$$

Similarly, it can be deduced that the DC side satisfies the following equation:

$$U_{dc} - (u_{pj} + u_{nj}) = 2L\frac{di_{Zj}}{dt} \tag{4}$$

According to Eqs. 3 and 4, the upper and lower bridge-arm voltages include the AC component and DC component, where the DC component is the same, and the AC component has the same amplitude and opposite phase. The DC-side voltage of the MMC is related to the sum of the upper and lower bridge-arm voltage, and the AC side voltage is related to the difference between the upper and lower bridge-arm voltage. Therefore, the required DC and AC output voltages can be obtained by varying the voltage of the upper and lower bridge arm using a specific control strategy.

For the line side, the MMC-based STATCOM can be viewed as a voltage source that has the same frequency as the voltage of the grid, but with a variable output voltage amplitude and phase. By adjusting the output voltage amplitude and phase to control the output current, the reactive power required by the grid is absorbed or transmitted, enabling the reactive power compensation for the grid to be completed. Figure 3 shows the equivalent circuit and working vector diagram of the STATCOM in the ideal situation. It can be seen from the figure that the phase difference between the current and voltage vector is 90° owing to the existence of the grid-connected reactor. Then the phase of the STATCOM output voltage u_{j0} and network voltage e_{sj} remains the same. In the capacitive condition, when $e_{sj} > u_{jo}$, the current vector is a 90° leading voltage, the STATCOM can be regarded as an inductance, and the reactive power output is negative in the capacitive condition. In the inductive condition, when $e_{sj} < u_{jo}$, the current vector is a 90° lagging voltage, the STATCOM can be considered a capacitance, and the reactive power output is positive.

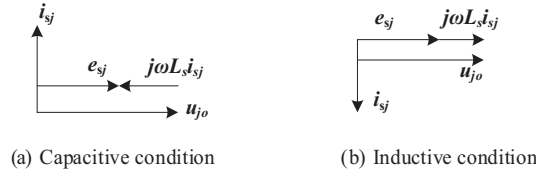(a) Capacitive condition   (b) Inductive condition

Figure 3. Working vector diagram of MMC-based STATCOM.

3. Modified instantaneous symmetrical components

3.1. Symmetrical component method and instantaneous value representation in phasor-time domain

Three-phase asymmetrical phasors can be decomposed into three groups of symmetrical phases using the symmetrical component method, that is, positive-, negative-, and zero-sequence components. In the present paper, the relationship between the three-phase asymmetrical phasor and its sequence components is illustrated using the example of a voltage phasor (with the basis reference of the phase voltage), as shown in Eqs. 5–7:

$$\begin{bmatrix} U_a^+ \\ U_b^+ \\ U_c^+ \end{bmatrix} = \frac{1}{3} \begin{bmatrix} 1 & a & a^2 \\ a^2 & 1 & a \\ a & a^2 & 1 \end{bmatrix} \begin{bmatrix} U_a \\ U_b \\ U_c \end{bmatrix} \tag{5}$$

$$\begin{bmatrix} U_a^- \\ U_b^- \\ U_c^- \end{bmatrix} = \frac{1}{3} \begin{bmatrix} 1 & a^2 & a \\ a & 1 & a^2 \\ a^2 & a & 1 \end{bmatrix} \begin{bmatrix} U_a \\ U_b \\ U_c \end{bmatrix} \tag{6}$$

$$U_0 = (U_a + U_b + U_c)/3, \tag{7}$$

where U_a, U_b, U_c are the three-phase voltage phasor; U_a^+, U_b^+, U_c^+ are the three-phase positive-sequence component; U_a^-, U_b^-, U_c^- are the three-phase voltage phasor; U_0 is the zero-sequence component; α is $e^{j2\pi/3}$.

Herein we present an example involving the use of a voltage positive-sequence component to analyze the representation of the instantaneous value of the phasor in the time domain. The positive-sequence phasor of

the three-phase voltage is expressed as follows in the form of real and imaginary parts:

$$\begin{cases} U_a^+ = ReU_a^+ + jImU_a^+ \\ U_b^+ = ReU_b^+ + jImU_b^+ \\ U_c^+ = ReU_c^+ + jImU_c^+ \end{cases} \tag{8}$$

When the phasor is rotated at an angular velocity w in the 2D orthogonal coordinate system $\alpha\beta$, the projection on any of the axes of this phasor can be defined as its instantaneous value. In this case, the β axle is selected; thus, the imaginary part of the voltage phasor in Eq. 8 refers to the instantaneous value of each phasor.

Eq. 8 is substituted into Eq. 5 and it is then expanded in the form of real and imaginary parts:

$$\begin{bmatrix} ReU_a^+ \\ ReU_b^+ \\ ReU_c^+ \end{bmatrix} = \frac{1}{3} \begin{bmatrix} 1 & 0 & -\frac{1}{2} & -\frac{\sqrt{3}}{2} & -\frac{1}{2} & \frac{\sqrt{3}}{2} \\ -\frac{1}{2} & \frac{\sqrt{3}}{2} & 1 & 0 & -\frac{1}{2} & -\frac{\sqrt{3}}{2} \\ -\frac{1}{2} & -\frac{\sqrt{3}}{2} & -\frac{1}{2} & \frac{\sqrt{3}}{2} & 1 & 0 \end{bmatrix} \begin{bmatrix} ReU_a \\ ImU_a \\ ReU_b \\ ImU_b \\ ReU_c \\ ImU_c \end{bmatrix} \tag{9}$$

$$\begin{bmatrix} ImU_a^+ \\ ImU_b^+ \\ ImU_c^+ \end{bmatrix} = \frac{1}{3} \begin{bmatrix} 0 & 1 & \frac{\sqrt{3}}{2} & -\frac{1}{2} & -\frac{\sqrt{3}}{2} & -\frac{1}{2} \\ -\frac{\sqrt{3}}{2} & -\frac{1}{2} & 0 & 1 & \frac{\sqrt{3}}{2} & -\frac{1}{2} \\ \frac{\sqrt{3}}{2} & -\frac{1}{2} & -\frac{\sqrt{3}}{2} & -\frac{1}{2} & 0 & 1 \end{bmatrix} \begin{bmatrix} ReU_a \\ ImU_a \\ ReU_b \\ ImU_b \\ ReU_c \\ ImU_c \end{bmatrix} \tag{10}$$

As can be seen from the above two equations, as long as the instantaneous value of the real and imaginary parts of the three-phase voltage phasor is detected in real time, the instantaneous value of the real and imaginary parts of the positive-sequence voltage phasor can be obtained.

3.2. Implementation of modified instantaneous symmetrical components with two sampling points

In the present paper, the time-domain instantaneous component of each voltage phasor is determined by employing the two-point sampling method with the use of the characteristics of the fundamental-wave sinusoidal quantity. The sampling period is set as T_s, t_1 is the last sampling time, and t_2 is the current sampling time, and so the corresponding voltage u representing the instantaneous value of t_1 and t_2 is expressed as follows:

$$u_1 = U_m \sin(\alpha - wT_s) \tag{11}$$

$$u_2 = U_m \sin\alpha, \tag{12}$$

where U_m- voltage peak; $\alpha-$ current-voltage phase angle; w$-$ angular velocity.

The real and imaginary parts of the voltage phasor can be obtained using Eqs. 13 and 14 as follows:

$$ReU = (U_2 \cos wT_s - U_1)/\sqrt{2}\sin wT_s \tag{13}$$

$$ImU = U_m \sin\alpha/\sqrt{2} = U_2/\sqrt{2} \tag{14}$$

It can be seen from Eqs. 13 and 14 that when the sampling period T_s is determined the voltage phase U can be determined by two consecutive sampling points because wT_s is a definite value (because T_s is very small, when the frequency of the fundamental wave of the grid fluctuates over a small range the influence on wT_s is negligible).

The three-phase voltage phasor is expressed and sorted in the form of real and imaginary parts according to Eqs. 15 and 16, respectively.

$$\begin{bmatrix} ReU_a \\ ImU_a \\ ReU_b \\ ImU_b \\ ReU_c \\ ImU_c \end{bmatrix} = \frac{1}{\sqrt{2}} \begin{bmatrix} \frac{-1}{\sin wT_s} & ctanwT_s & 0 & 0 & 0 & 0 \\ 0 & 1 & 0 & 0 & 0 & 0 \\ 0 & 0 & \frac{-1}{\sin wT_s} & ctanwT_s & 0 & 0 \\ 0 & 0 & 0 & 1 & 0 & 0 \\ 0 & 0 & 0 & 0 & \frac{-1}{\sin wT_s} & ctanwT_s \\ 0 & 0 & 0 & 0 & 0 & 1 \end{bmatrix} \begin{bmatrix} U_{a1} \\ U_{a2} \\ U_{b1} \\ U_{b2} \\ U_{c1} \\ U_{c2} \end{bmatrix} \tag{15}$$

Here $U_{a1}, U_{a2}, U_{b1}, U_{b2}, U_{c1}, U_{c2}$ are two consecutive instantaneous value sampling points for the three-phase voltage.

Eq. 15 is substituted into Eqs. 9 and 10 and it is sorted as follows:

$$\begin{bmatrix} ReU_a^+ \\ ReU_b^+ \\ ReU_c^+ \end{bmatrix} = \frac{1}{3\sqrt{2}} \begin{bmatrix} \frac{-1}{\sin wT_s} & ctanwT_s & \frac{1}{2\sin wT_s} & \frac{-ctanwT_s-\sqrt{3}}{2} & \frac{1}{2\sin wT_s} & \frac{-ctanwT_s+\sqrt{3}}{2} \\ \frac{1}{2\sin wT_s} & \frac{-ctanwT_s+\sqrt{3}}{2} & \frac{-1}{\sin wT_s} & ctanwT_s & \frac{1}{2\sin wT_s} & \frac{-ctanwT_s-\sqrt{3}}{2} \\ \frac{1}{2\sin wT_s} & \frac{-ctanwT_s-\sqrt{3}}{2} & \frac{1}{2\sin wT_s} & \frac{-ctanwT_s+\sqrt{3}}{2} & \frac{-1}{\sin wT_s} & ctanwT_s \end{bmatrix} \begin{bmatrix} U_{a1} \\ U_{a2} \\ U_{b1} \\ U_{b2} \\ U_{c1} \\ U_{c2} \end{bmatrix} \tag{16}$$

$$\begin{bmatrix} ImU_a^+ \\ ImU_b^+ \\ ImU_c^+ \end{bmatrix} = \frac{1}{3\sqrt{2}} \begin{bmatrix} 0 & 1 & \frac{-\sqrt{3}}{2\sin wT_s} & \frac{\sqrt{3}ctanwT_s-1}{2} & \frac{-\sqrt{3}}{2\sin wT_s} & \frac{-\sqrt{3}ctanwT_s-1}{2} \\ \frac{\sqrt{3}}{2\sin wT_s} & \frac{-\sqrt{3}ctanwT_s-1}{2} & 0 & 1 & \frac{-\sqrt{3}}{2\sin wT_s} & \frac{\sqrt{3}ctanwT_s-1}{2} \\ \frac{-\sqrt{3}}{2\sin wT_s} & \frac{\sqrt{3}ctanwT_s-1}{2} & \frac{\sqrt{3}}{2\sin wT_s} & \frac{-\sqrt{3}ctanwT_s-1}{2} & 0 & 1 \end{bmatrix} \begin{bmatrix} U_{a1} \\ U_{a2} \\ U_{b1} \\ U_{b2} \\ U_{c1} \\ U_{c2} \end{bmatrix} \tag{17}$$

According to Eqs. 16 and 17, the voltage phasor of the current moment can be obtained by using the two-point sampling method to continuously collect six sets of data. Meanwhile, the amplitude, phase angle, and sine and cosine function of the positive-sequence components of the voltage are conveniently obtained by using phase A as an example.

$$U_a^+ = \sqrt{(ReU_a^+)^2 + (ImU_a^+)^2} \tag{18}$$

$$\alpha_{U_a^+} = arctg(ImU_a^+/ReU_a^+) \tag{19}$$

$$\sin\alpha_{U_a^+} = ImU_a^+/U_a^+ \tag{20}$$

$$\cos \alpha_{U_a^+} = ReU_a^+/U_a^+ \tag{21}$$

The instantaneous expression of the real and imaginary parts of the negative- and zero-sequence components of the voltage can be obtained according to the above derivation process.

4. Control method

4.1. Fixed DC voltage control

In an ideal situation, there should be only a reactive power exchange between the modular multilevel STATCOM and the grid, and the DC-side voltage should be constant. However, in actual cases, owing to the loss inside the modular multilevel STATCOM device, the DC-side voltage must change. The main part of the modularized multilevel STATCOM is the MMC. The normal operation of the MMC can be directly affected when the voltage loses stability on the DC side. Therefore, it is necessary to conduct voltage stability control on the DC side of the modularized multilevel STATCOM to ensure the normal operation of the device. Changes in the DC-side voltage will cause the exchange of active power. Therefore, the voltage on the DC side is balanced by the control of the active current output from the STATCOM. In an actual implementation, the error signal can be sent to the PI link for nonstatic tracking by comparing it with the reference value after detecting the DC-side voltage, that is,

$$i_{sd}^{*+} = K_p(U_{dref} - U_{dc}) + K_i \int (U_{dref} - U_{dc})\mathrm{d}t, \tag{22}$$

where K_p and K_i are respectively the proportion and integration coefficients of the PI link and U_{dref} refers to the DC voltage instruction value.

4.2. DC voltage balancing control

In MMC systems, the DC capacitance-voltage balance of each submodule is based on the normal and stable work of MMC systems. Because of the reference positive direction of the current, the upper and lower bridge arms are different in the j phase, and it is necessary to consider the influence of the current direction of the bridge arm when introducing the capacitance-voltage balance control of the submodule. The basic principle is to multiply the bridge-arm current by the difference between the submodule capacitance-voltage value u_{cji} and the average DC voltage of the bridge arm u_{cj} after passing the proportional controller. Thus, the capacitance-voltage balance control component V_{Aji^*} of the submodule is generated. Then this component is added to the modulating wave to effectively realize the balance control of the capacitance voltage of the submodule. Thus, the capacitance-voltage balance control correction component V_{Aji^*} of the submodule satisfies

$$V_{Aji^*} = \begin{cases} -K_{p1} = (\overline{u}_{cj} - u_{Cji})i_{pj}(i=1,2,3...N) \\ K_{p1} = (\overline{u}_{cj} - u_{Cji})i_{nj}(i=N+1,N+2,N+3...2N) \end{cases} \tag{23}$$

For the i_{th} submodule in the upper bridge arm, if the capacitance-voltage value u_{cji} is greater than its reference value, when the bridge-arm current $i_{pj} > 0$ the output voltage balance-control correction component $V_{Aji^*} > 0$. Accordingly, the capacitance of the submodule releases the active power, that is, the capacity discharge, and the capacitance voltage of the submodule decreases. In contrast, when the bridge-arm current $i_{pj} < 0$, the output voltage balance control correction component $V_{Aji^*} < 0$. Accordingly, the capacitance

of the submodule absorbs the active power, that is, the capacity charge, and the capacitance voltage of the submodule increases, and so on. In this paper, the capacitance voltage balance control correction component of the submodule can be obtained by combining the reference voltage value of the capacitance voltage of different bridge arms and the direction of the bridge-arm current. The component directly affects the release and absorption of energy stored in the DC current capacity of the submodule, thus determining the submodule voltage and helping to realize the voltage balance of the submodule.

4.3. Current decoupling control

In the present paper, the DC current control method is adopted to control the internal power flow in the MMC system by controlling the three-phase current on the AC side. Compared with the MMC used in flexible DC transmission, the MMC-STATCOM does not lead to the DC side and so there is neither a zero-sequence path nor a current. Therefore, the MMC system is decomposed into a three-phase symmetrical positive-sequence system model and a negative-sequence system model, and the two systems are respectively controlled. The respective decoupling mathematical models can be described as follows:

$$
\begin{cases}
U_{od}^+ = e_{sd}^+ + wL_s i_{sq}^+ - [K_{p11}(i_{dref} - i_{sd}^+) + K_{i11}\int(i_{sd}^{+*} - i_{sd}^+)\mathrm{d}t] \\
U_{oq}^+ = e_{sq}^+ - wL_s i_{sd}^+ - [K_{p12}(i_{sq}^{+*} - i_{sq}^+) + K_{i12}\int(i_{sq}^{+*} - i_{sq}^+)\mathrm{d}t]
\end{cases}
\tag{24}
$$

$$
\begin{cases}
U_{od}^- = e_{sd}^- - wL_s i_{sq}^- - [K_{p13}(i_{sd}^{-*} - i_{sd}^-) + K_{i13}\int(i_{sd}^{-*} - i_{sd}^-)\mathrm{d}t] \\
U_{oq}^- = e_{sq}^- + wL_s i_{sd}^- - [K_{p14}(i_{sq}^{-*} - i_{sq}^-) + K_{i14}\int(i_{sq}^{-*} - i_{sq}^-)\mathrm{d}t]
\end{cases}
\tag{25}
$$

Among them, e_{sd}^+, e_{sq}^+, e_{sd}^-, and e_{sq}^- are the dq components of the positive- and negative-sequence components of the AC side voltage, and i_{sd}^+, i_{sq}^+, i_{sd}^-, and i_{sq}^- are the dq components of the positive- and negative-sequence components of the grid-connected current.

4.4. Circulating current suppression method

In MMC systems, the common DC bus transmits both active power and reactive power through the DC capacitance in the submodule. However, owing to the incomplete capacitance of each submodule, there are different instantaneous values of the three-phase bridge-arm voltage, resulting in circulation. Circulation is the mechanism responsible for energy exchange and DC capacitance voltage control, and it will distort the AC current flowing through the bridge arm, causing increased system loss. In the present study, a negative-sequence double-frequency circulation suppressor was designed, and it is shown in Figure 4. Its basic working principle is to calculate the phase circulation i_{zj} by the j phase bridge-arm current, and to obtain the dq component i_{zd} and i_{zq} in the negative-sequence double-frequency rotation coordinate system of the three-phase circulation using the abc/dq transformation. After comparison with the reference value, the circulation restraint three-phase voltage corrections V_{ZA}^*, V_{ZB}^*, and V_{ZC}^* are obtained after passing the PI controller through decoupling control.

4.5. Overall control

By integrating the DC voltage stability control, DC voltage balance control, positive- and negative-sequence current decoupling control, and circulation suppression control, the modulating wave signal of each power device can be obtained by combining the linear voltage signals of each control link. Figure 5 shows the overall control
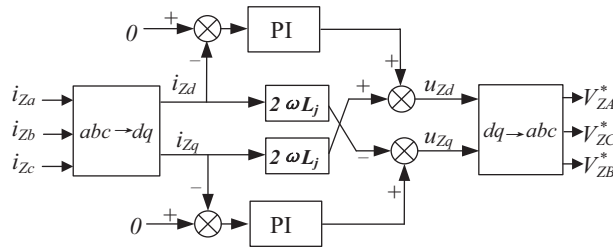
Figure 4. Negative-sequence double-frequency circulation suppressor of MMC.

structure of the MMC. Positive- and negative-sequence current decoupling control can achieve positive- and negative-sequence modulating wave components u_j^+ and u_j^- of each phase bridge-arm module. The negative-sequence double-frequency circulation suppressor can acquire u_{zj}^*, and the DC voltage balance control can obtain the modulating wave correction u_{Aji}^* of each unit. The modulating wave of each unit can be generated by adding the four modulating wave components. The present paper adopts the carrier phase-shift sinusoidal pulse width modulation (CPS-PWM) strategy as the modulation method, and the lower switching frequency can be used to achieve a higher equivalent switching frequency [15,16]. If each bridge arm has N submodules, the single-phase output voltage will have 2N+1 level. The method of PI parameter design can be referred to [17,18].
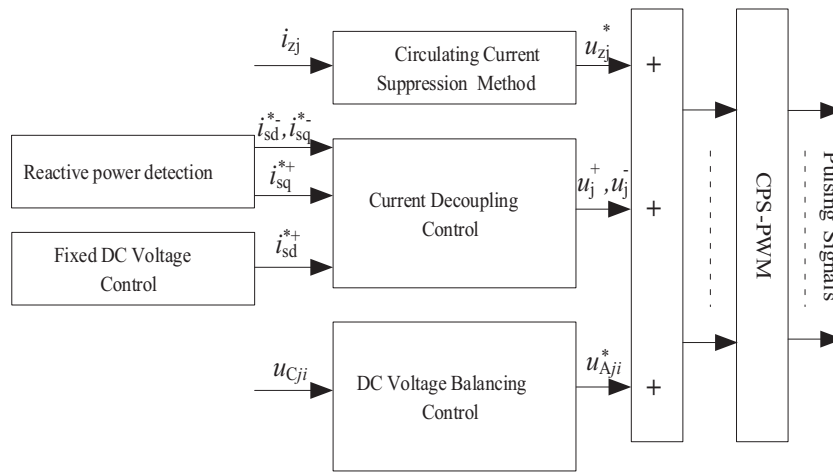

Figure 5. Overall control block diagram of MMC.

5. Simulation and experiment study

5.1. Simulation verification of modified instantaneous symmetrical components

In this section, MATLAB is used to establish a simulation model that performs simulation verification for modified instantaneous symmetrical components. The initial state is set as three-phase voltage symmetry, the base wave frequency f_0 is 50 Hz, and the sampling period Ts is 12.8 kHz. The simulation time is set to 0.1 s. During the period t = 0.02 s-0.04 s, there is a failure of simulation voltage drop. During the period t = 0.06 s-0.1 s, the voltage of phase C is disconnected, and there is a three-phase asymmetrical transient fault of simulation voltage. The specific simulation waveform is as shown in Figure 6.

In Figure 6, the waveforms from top to bottom are three-phase voltages u_a, u_b, and u_c; three-phase positive-sequence voltage components u_a^+, u_b^+, and u_c^+; three-phase negative-sequence voltage components u_a^-,
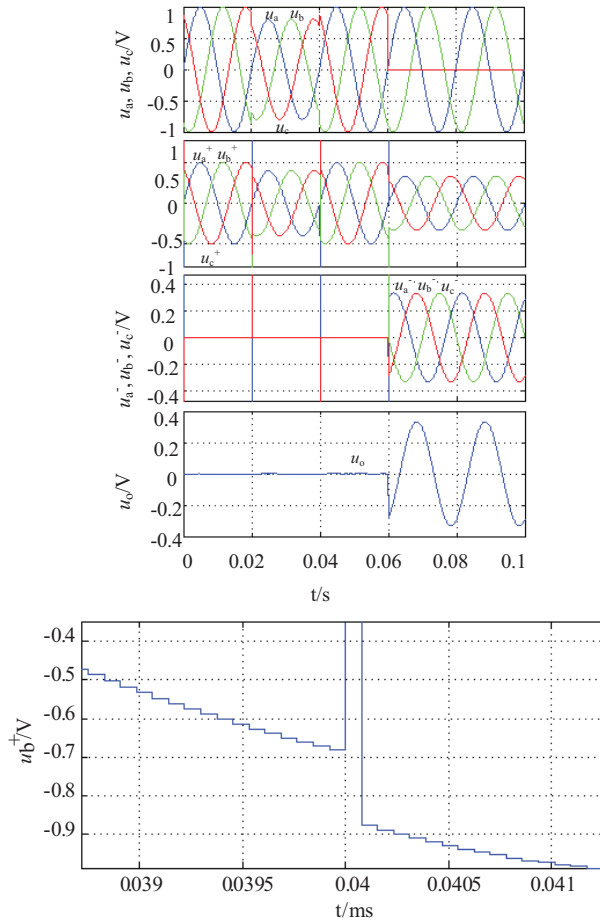
Figure 6. Simulation waveform based on modified instantaneous symmetrical component method.

u_b^-, and u_c^-; and zero-sequence component u_0. As can be seen from the figure, the three-phase voltage waveform is symmetrical when $t < 0.06s$. Therefore, the corresponding three-phase voltage positive-sequence component waveform is entirely consistent with the three-phase voltage waveform, while the three-phase negative-sequence voltage and zero-sequence voltage are zero. At t = 0.06 s, the phase C voltage is suddenly disconnected, i.e. u_c = 0, owing to the two-point sampling method, and only the transient transition time of one sampling period $(1/T_s = 78.125e^{-6}s)$ is required, and the sequence components of the voltage can reach the steady state. In the steady state, the negative-sequence and zero-sequence components of the voltage are not zero because of the three-phase asymmetry.

In addition, as can be seen from the figure, during the transition of a sampling period, each sequence voltage changes suddenly. The local amplification of the transition process is as shown in Figure 6 (this is a case of the positive-sequence voltage of the B phase). The major reason is that when the voltage changes suddenly, the increase in u_2 causes an increase in the molecular difference. Compared with the sharp increase in ReU arising from denominator small data $\sin(wT_s)$, the large difference results in a sudden change in the sequence components of the voltage. In practical engineering applications, the data are limited to data processing. Furthermore, when the voltage is going through normal changes rather than short-circuit or open-circuit or has other limit fault states, it will not cause a large voltage change.

5.2. Simulation verification of MMC-based STATCOM

The parameter design of the specific MMC device is not the focus of this paper; interested readers can refer to [19].

When the system is connected to a resistance capacity load, the simulation waveform of the modularized multilevel STATCOM reactive compensation condition is as shown in Figure 7. In the simulation model, the main circuit parameters are as shown in Table 1, with a three-phase symmetrical load. The load resistance is 100 Ω, the load capacitance is 250μF, and the simulation time is 0.2 s.

Table 1. Main parameters of the simulation model of reactive compensation in equilibrium condition.

Parameter Name	Parameter Value
Effective value U_s of grid line voltage	10 kV
Bridge-arm inductance L_a	10 mH
Inductance L_s on AC side	5 mH
Capacitance value of submodule C	470 μF
Capacitance voltage reference value Ucref of submodule	4 kV
Number of bridge-arm modules N	4
Carrier frequency f_c	2kHz

Figure 7a shows the phase voltage and current waveform diagram of the grid. As can be seen from the figure, the grid current is ahead of the grid voltage before the STATCOM is put into operation owing to the presence of the resistance capacity load. Because of the role of the STATCOM output compensation current, the phase voltage and current are always in the same phase.

Figure 7b shows the phase voltage and STATCOM output for the phase-compensation current waveform diagram. As can be seen, when the STATCOM is put into operation after 0.1 s, the current output from it lags behind the grid voltage in order to realize compensation for the leading current in the grid. Meanwhile, as can be seen from Figures 7a and 7b after the input, the STATCOM has completed the compensation for the grid current after 0.02 s, i.e. a cycle with a fast response speed. Figure 7c shows the power-factor waveform diagram. The system power factor is 0.62 before the input of the STATCOM. However, it is significantly improved to 0.99 after the input of the STATCOM, and the voltage and current are basically in the same phase, thus verifying the validity of the proposed STATCOM control strategy.

Figure 7d is the capacitance voltage waveform of the phase A submodule. Before 0.1 s, the capacitance voltage of the submodule is near the reference value, and the circulation is smaller because the STATCOM is not input. When the STATCOM is input, after a temporary stability period, the capacitance voltage may still fluctuate around the reference value.

5.3. Experiment verification of MMC-based STATCOM

In order to verify the effectiveness and feasibility of the proposed control method, the present study constructs the MMC-based STATCOM, as shown in Figure 8 and Table 2, and carries out the test verification. The reactive load used in the experiment is a purely inductive load of 30 kVar, and the experimental waveform is as shown in Figure 9.
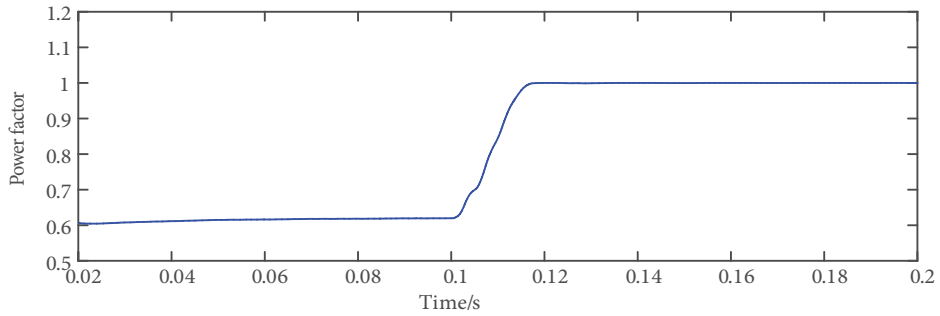
Figure 9(a) shows the experimental waveform of the system line voltage e_{ab} (waveform 1), the device's phase A output voltage u_{Ca} (waveform 2), and output current i_{Ca} (waveform 3). Owing to the three-phase
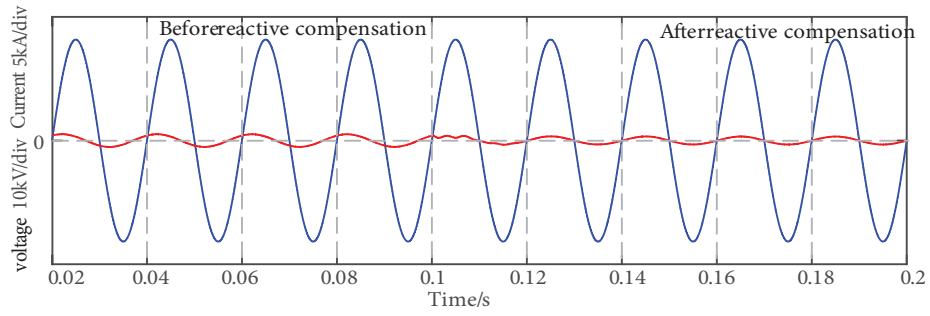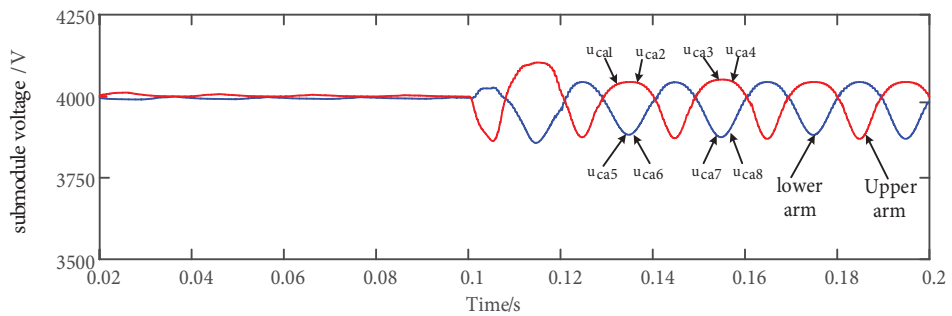
(a) Voltage of phase A and current
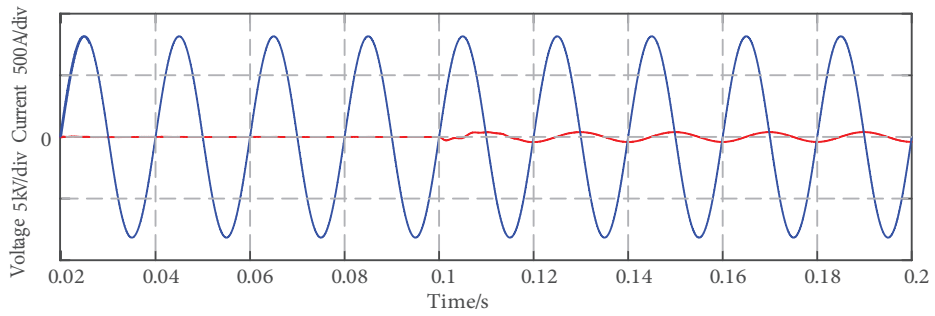
(b) Voltage of phase A and STATCOM output for phase A compensation current

(c) Power factor

(d) Phase A submodule capacitance voltage

Figure 7. Modularized multilevel STATCOM reactive compensation condition.

symmetry of the device, only the phase A voltage and current experimental waveform are given here. As can be seen from the figure, u_{Ca} lags e_{ab} by a phase angle of nearly 30°, and i_{Ca} lags u_{Ca} by nearly 90° degrees, satisfying the basic principle of reactive power. In addition, the required output voltage of the device is small
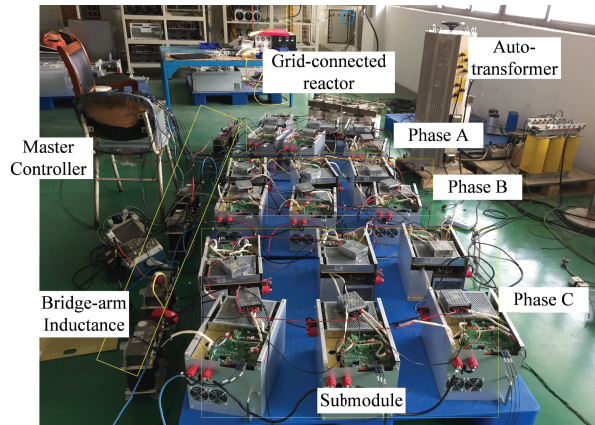
Figure 8. Experimental platform

(a) Experimental waveform diagram of e_{ab}, u_{Ca}, and i_{Ca}

(b) Experimental waveform diagram of i_{La} and i_{Ca}

(c) Experimental waveform diagram of i_{Ca}, i_{Cb}, and i_{Cc}

(d) Experimental waveform diagram of u_{Ca} and i_{Ca} inversion starting transient
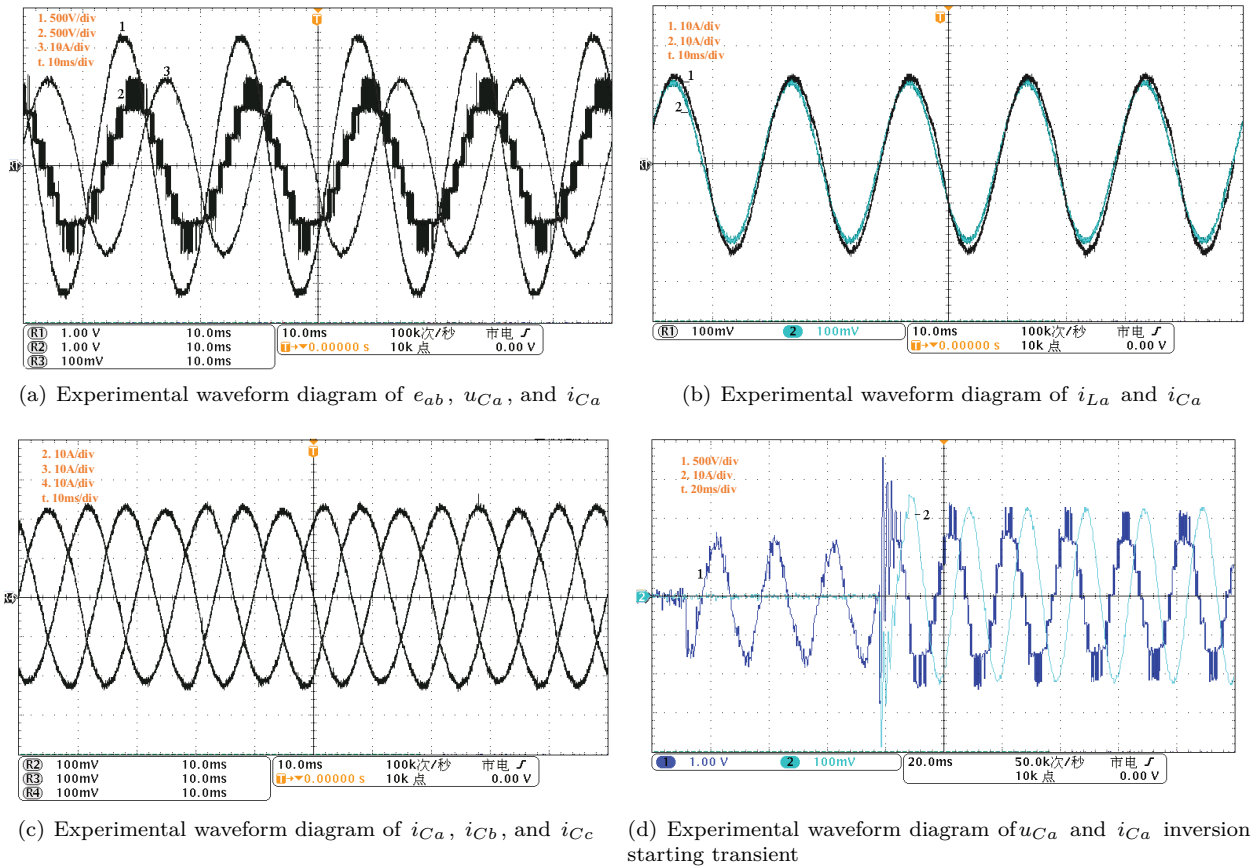
Figure 9. Reactive load compensation experiment.

owing to the small output power capacity, showing the low output voltage level of the device, only 9.

Figure 9(b) shows the experimental waveform diagram of the phase A load current i_{La} (waveform 2) and the device's output compensation current i_{Ca} (waveform 1). It can be seen that i_{Ca} can track i_{La} in real time as well as the output reactive power to the system in order to realize reactive compensation. In addition, the phase of i_{Ca} lags behind that of i_{La}, which is a comprehensive tracking error caused by data detection, filtering, and tracking control.

Table 2. Parameters of the simulation model.

Parameter Name	Parameter Value
Effective value U_s of grid line voltage	1140 kV
Bridge-arm inductance L_a	10 mH
Inductance L_s on AC side	15 mH
Capacitance value of submodule C	5600 μF
Capacitance voltage reference value U_{cref} of submodule	350 V
Number of bridge-arm modules N	3
Carrier frequency f_c	2 kHz

Figure 9(c) shows the experimental waveform diagram of the three-phase output current i_{Ca}, i_{Cb}, i_{Cc} and Figure 9(d) shows the captured transient waveform diagram of the output voltage (waveform 1) and current (waveform 2) of the starting stage of the device. Because the image capture and displayed time-axis scale is larger, the display image is rougher. As can be seen from the figure, the first three cyclic waves of the voltage waveform are the voltage applied to the device after the device closes and before compensation starts. Since that instance in time, the compensation device starts operation and the output voltage reaches a stable state through the transient oscillation process for about one quarter of a cycle. The compensation current is 0 until the device compensation starts, and the compensation instruction current is tracked quickly after the compensation starts.

The experiment of Figure 10 is to simulate the tracking compensation ability of the MMC-based STATCOM when the impulsive reactive load changes abruptly. Two groups of reactive load 30 kVar and 60 kVar are set up in the experiment. First, 30 kVar is put into operation, and at a certain time 60 kVar is put into operation to simulate the sudden change in reactive load. Because of the three-phase symmetry and space limitation, only the experimental waveforms of phase A are given here.
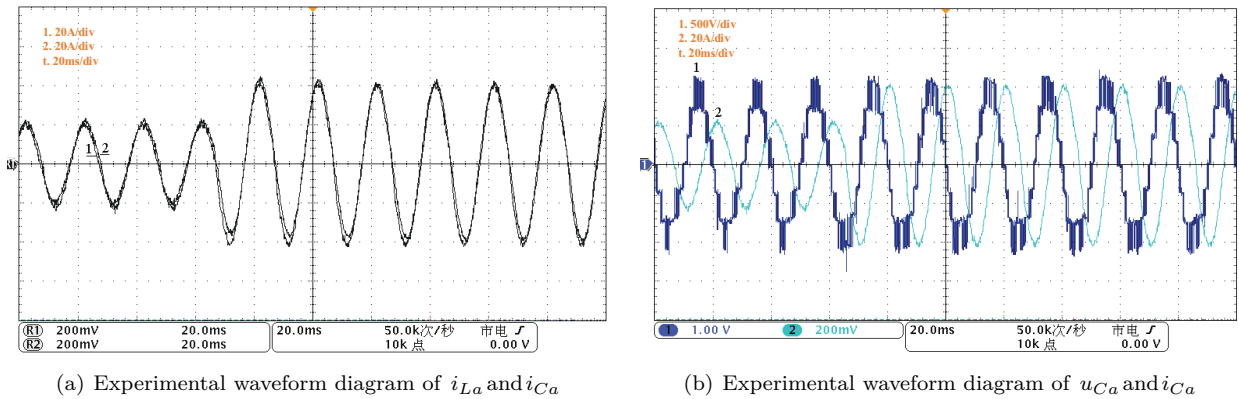

(a) Experimental waveform diagram of i_{La} and i_{Ca} (b) Experimental waveform diagram of u_{Ca} and i_{Ca}

Figure 10. Impulsive reactive power load compensation experiment.

Figure 10(a) shows the experimental waveform of load current i_{La} (waveform 1) and device output compensation current i_{Ca} (waveform 2). It can be seen that i_{Ca} can track and compensate i_{La} in real time when the reactive load changes abruptly. Figure 10(b) shows the waveforms of u_{Ca} (waveform 1) and i_{Ca} (waveform 2). It can be seen from the graph that when the load suddenly changes the output voltage of the device transits to a stable state through a transient process of about half a cycle. The observation of u_{Ca}

shows that although the level number does not increase, the number of peak level pulses increases significantly, which indicates that the effective value of u_{Ca} increases, which is caused by the increase in reactive power compensation capacity.

Figure 11 shows the test waveform of the device for unbalanced reactive compensation. The experimental load is an inductive reactive power of 30 kVar and resistance 30 Ω. The resistance is strung into the inductance of the phase A line, thus simulating the unbalanced three-phase load. Figure 11(a) shows the waveform of the three-phase asymmetric load current i_{La}, i_{Lb}, and i_{Lc}. Figure 11(b) shows the three-phase output compensation current i_{Ca} (waveform 1), i_{Cb} (waveform 2), and i_{Cc} (waveform 3) waveforms of the device. Figure 11(c) shows the current i_{afp}^{+} (waveform 1), i_{bfp}^{+}(waveform 2), and i_{cfp}^{+} (waveform 3) waveforms of the compensated three-phase system. Therefore, the three-phase current is almost symmetrical.

(a) Experimental waveform diagram of i_{La}, i_{Lb}, and i_{Lc}

(b) Experimental waveform diagram of i_{Ca}, i_{Cb}, and i_{Cc}

(c) Experimental waveform diagram of i_{afp}^{+}, i_{bfp}^{+}, and i_{cfp}^{+}

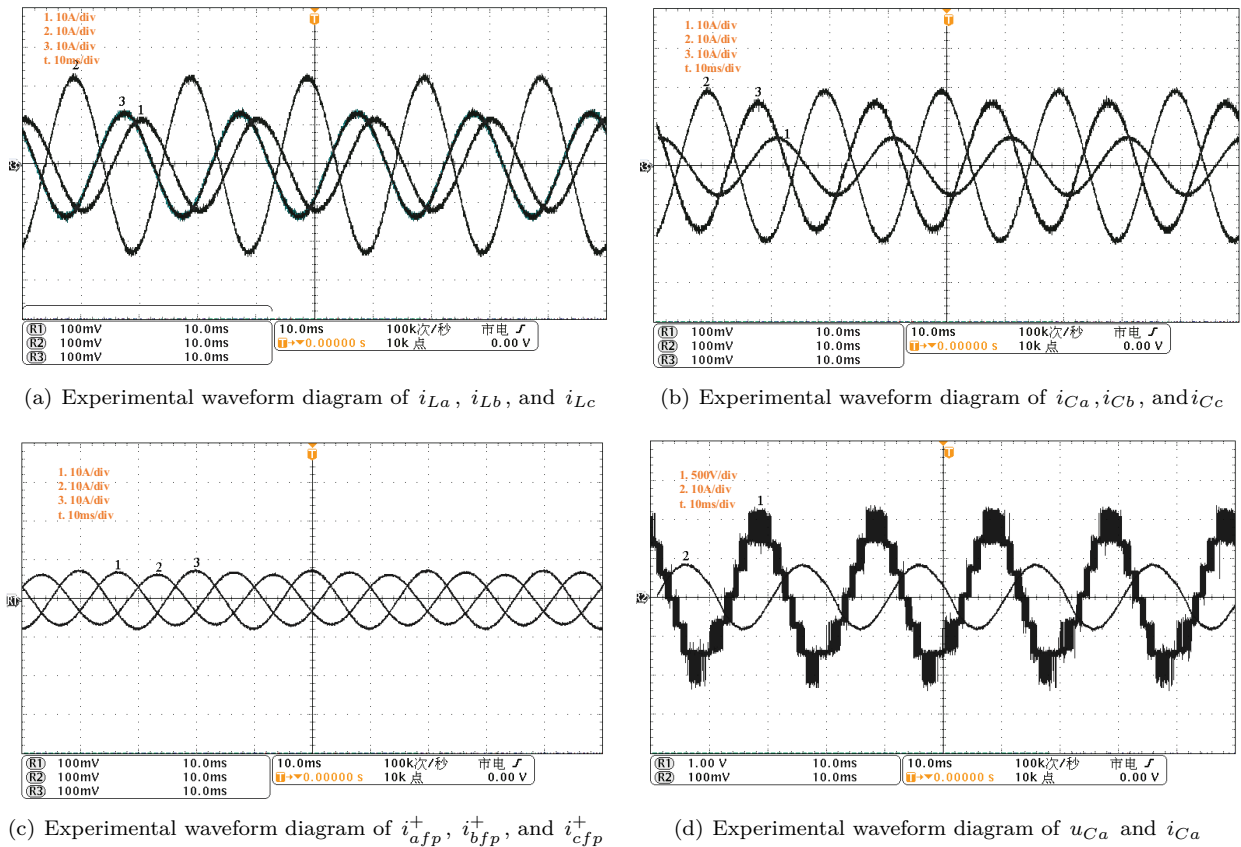(d) Experimental waveform diagram of u_{Ca} and i_{Ca}

Figure 11. Three-phase unbalanced load compensation experiment.

According to the experimental waveform diagram in Figure 10, the device can effectively compensate the reactive power and negative-sequence components in the three-phase asymmetrical load, and so the system can only provide the positive-sequence active component of the three-phase fundamental wave. Figure 11(d) shows the experimental waveform diagram of the output voltage u_{Ca} and the output current i_{Ca} of phase A of the device. As can be seen from the figure, the device also outputs a negative-sequence compensation current in addition to the reactive-power compensation current.

6. Conclusion

In this paper, we proposed a modified instantaneous symmetrical component transformation method for an MMC-based STATCOM to further design the control method of a multi-DC voltage, positive- and negative-sequence current, and the circulation suppression of an MMC-based STATCOM. The proposed method can detect the sequence components in three phases asymmetrically in real time, and with fast dynamic response speed within several sampling points. The proposed control method can control the compensation currents within one quarter of a power frequency cycle. The simulation and experimental results show that it can detect and control the positive- and negative-sequence reactive components that are required by the device quickly and accurately in order to realize the real-time reactive compensation of MMC-based STATCOMs.

References

[1] Robbins BA, Domínguez-García AD. Optimal reactive power dispatch for voltage regulation in unbalanced distribution systems. IEEE Transactions on Power Systems 2016; 31 (4): 2903-2913.

[2] Czarnecki LS, Haley PM. Unbalanced power in four-wire systems and its reactive compensation. IEEE Transactions on Power Delivery 2015; 30 (1): 53-63.

[3] Lee SY, Wu CJ. On-line reactive power compensation schemes for unbalanced three phase four wire distribution feeders. IEEE Transactions on Power Delivery 1993; 8 (4): 1958-1965.

[4] Tan YL. Analysis of line compensation by shunt-connected FACTS controllers: a comparison between SVC and STATCOM. IEEE Power Engineering Review 1999; 19 (8): 57-58.

[5] Pereira MMR, Ferreira CMM, Barbosa FM. Comparative study of STATCOM and SVC performance on dynamic voltage collapse of an electric power system with wind generation. IEEE Latin America Transactions 2014; 12 (2): 138-145.

[6] Tang Y, He H, Ni Z, Wen J, Huang T. Adaptive modulation for DFIG and STATCOM with high-voltage direct current transmission. IEEE Transactions on Neural Networks and Learning Systems 2016; 27 (8): 1762-1772.

[7] Haw LK, Dahidah MSA, Almurib HAF. SHE–PWM cascaded multilevel inverter with adjustable DC voltage levels control for STATCOM applications. IEEE Transactions on Power Electronics 2014; 29 (12): 6433-6444.

[8] Schön A, Hofmann V, Bakran MM. Optimisation of the HVDC auto transformer by using hybrid MMC modulation. IET Power Electronics 2018; 11 (3): 468-476.

[9] Lyu J, Cai X, Amin M, Molinas M. Sub-synchronous oscillation mechanism and its suppression in MMC-based HVDC connected wind farms. IET Generation, Transmission and Distribution 2018; 12 (4): 1021-1029.

[10] Bi T, Wang S, Jia K. Single pole-to-ground fault location method for MMC-HVDC system using active pulse. IET Generation, Transmission and Distribution 2018; 12 (2): 272-278.

[11] Kontos E, Tsolaridis G, Teodorescu R, Bauer P. High order voltage and current harmonic mitigation using the modular multilevel converter STATCOM. IEEE Access 2017; 5: 16684-16692.

[12] Strezoski VC. Advanced symmetrical components method. IET Generation, Transmission and Distribution 2011; 5 (8): 833-841.

[13] Ji FF, Khan MM, Chen C. Static var compensator based on rolling synchronous symmetrical component method for unbalance three-phase system. In: 2005 IEEE International Conference on Industrial Technology; Hong Kong; 2005. pp. 621-626.

[14] Elbouchikhi E, Choqueuse V, Feld G, Amirat Y, Benbouzid M. A symmetrical components-based load oscillation detection method for closed-loop controlled induction motors. In: 2017 IECON - 43rd Annual Conference of the IEEE Industrial Electronics Society; Beijing, China; 2017. pp. 8047-8052.

[15] Bau DF, Silva GSD, Pinheiro H, Grigolettol FB. PD modulation strategy for modular multilevel converters. In: IEEE International Conference on Industry Applications; Curitiba, Brazil; 2017. pp. 1-6.

[16] Singh M, Agarwal A, Kaira N. Performance evaluation of multilevel inverter with advance PWM control techniques. In: IEEE 5th International Conference on Power Electronics (IICPE); Delhi, India; 2012. pp. 1-6.

[17] Zhong Y, Roscoe N, Holliday D, Lim TC, Finney SJ. High-efficiency MOSFET-based MMC design for LVDC distribution systems. IEEE Transactions on Industry Applications 2017; 54 (1): 321-334.

[18] Moon JW, Kim CS, Park JW, Kang DW, Kim JM. Circulating current control in MMC under the unbalanced voltage. IEEE Transactions on Power Delivery 2013; 28 (3): 1952-1959.

[19] Barnklau H, Gensior A, Bernet S. Submodule capacitor dimensioning for modular multilevel converters. IEEE Transactions on Industry Applications 2014; 50 (3): 1915-1923.